Hofmann-like frameworks $Fe(2\text{-methylpyrazine})_n[M(CN)_2]_2$ (M = Au, Ag): spin crossover defined by the precious metal

Sergii I. Shylin,[ab] Olesia I. Kucheriv,[ac] Sergiu Shova,[d] Vadim Ksenofontov,[e] Wolfgang Tremel,[e] Il'ya A. Gural'skiy*[ac]*

[a] Department of Chemistry, Taras Shevchenko National University of Kyiv, Volodymyrska 64, 01601 Kyiv, Ukraine.

[b] Department of Chemistry – Ångström Laboratory, Uppsala University, PO Box 523, 75120 Uppsala, Sweden

[c] UkrOrgSyntez Ltd., Chervonotkatska 67, 02094 Kyiv, Ukraine

[d] Petru Poni Institute of Macromolecular Chemistry, Aleea Gr. Ghica Voda 41A, 700487 Iasi, Romania

[e] Institute of Inorganic and Analytical Chemistry, Johannes Gutenberg University of Mainz, Duesbergweg 10-14, 55128 Mainz, Germany

KEYWORDS: Spin crossover, cyanometalate, MOF, Iron, Mössbauer spectroscopy

ABSTRACT

Hofmann-like cyanometalates constitute a large class of spin-crossover iron(II) complexes with variable switching properties. However, it is not yet clearly understood, how the temperature and cooperativity of a spin transition are influenced by their structure. In this paper, we report the

synthesis and crystal structures of the metal-organic coordination polymers $\{Fe^{II}(Mepz)[Au^{I}(CN)_2]_2\}$ (**[Au]**) and $\{Fe^{II}(Mepz)_2[Ag^{I}(CN)_2]_2\}$ (**[Ag]**) (Mepz = 2-methylpyrazine) along with the characterization of their spin state behavior by variable temperature SQUID magnetometry and Mössbauer spectroscopy. The compounds are built of cyanoheterometallic layers, which are pillared by the bridging Mepz ligangs in **[Au]**, but separated in **[Ag]**. The complex **[Au]** exhibits an incomplete stepped spin transition as a function of temperature with T_{SCO1} = 170 K and T_{SCO2} = 308 K for the two subsequent steps, respectively. In contrast, the complex **[Ag]** attains the high-spin state over the whole temperature range. In the crystal structure of **[Ag]**, weak interlayer contacts Ag–π, Me–π and Ag–N are found that may be responsible for an unusual axial elongation of the FeN_6 polyhedra. We propose that this structural distortion contributes to the trapping of iron in its high-spin state.

INTRODUCTION

In coordination chemistry, determining and manipulating the spin state of a transition metal complex is essential to understand and tune its fundamental physical properties and chemical reactivity. A well-established spin crossover (SCO) model is that the entropy-driven conversion between the high-spin (HS) and low-spin (LS) states can be induced when the energy difference between these states is of the order of thermal energy.[1] More explicitly, the choice of ligands, their arrangement around the given metal ion and the resulting ligand field strength, alongside with long-range elastic interactions in the crystalline state, determine the stability of a certain spin configuration — and, consequently, SCO parameters.[2] In case of divalent iron, metal-to-ligand distances in the HS state (S = 2; $t_{2g}^4e_g^2$) are significantly larger than in the LS state (S = 2; $t_{2g}^6e_g^0$),

caused by the difference in the occupancy of anti-bonding molecular e_g orbitals. The ability of the lattice to tolerate the strains when switching between two spin states determines the degree of cooperativity in SCO materials.[3] Weakly cooperative systems usually exhibit gradual spin transitions, while in strongly cooperative systems SCO is abrupt and accompanied by a thermal hysteresis. However, strong accommodation of the lattice to the strains may also compromise the existence of SCO at all.[4] For example, certain materials where a spin transition might have been expected (since they have a local ligand environment) virtually identical to known SCO systems, still remain HS on cooling.[5] As a rule, HS forms of these materials exhibit greater structural distortions, which would require structural changes upon transition to the LS state, impossible for a rigid solid lattice.

Within the realm of iron(II) SCO complexes, the Hofmann-like clathrate compounds, where cyanometalate moieties $[M(CN)_{2n}]^{n-}$ (M = Cu, Ag, Au, n = 1; M = Ni, Pd, Pt, n = 2) link octahedrally coordinated Fe^{II} ions to form extended network structures, are among the most suitable materials for practical applications and fundamental studies.[6] Kitazawa *et al.* were first to report the spin transition in the 2D coordination polymer $[Fe^{II}(pyridine)_2Ni^{II}(CN)_4]$ with T_{SCO} = 190 K.[7] Efforts to enhance the cooperative interactions between SCO centers led to the development of 3D Hofmann-like MOFs by employing diazine ligands — pyrazine and pyrimidine — with the main contribution to this domain made by the Real group.[8] The most notable example $[Fe^{II}(pyrazine)Pt^{II}(CN)_4]$ with hysteretic SCO around room temperature was successfully used to design prototypes of chemical sensors and pressure sensors, prepared as nanoparticles and thin films, used to create composite materials, *etc*.[9] Complexes with SCO supported by the pyrimidine bridge $\{Fe(pmd)_2[M^I(CN)_2]_2\}$ (M^I = Au, Ag, Cu) were also elaborated successfully.[8c,d] The third remaining diazine-type ligand, pyridazine, was found to bind Fe^{II} in a pyridine manner forming

separated $[Fe^{II}(pyridazine)_2M^{II}(CN)_4]$ (M^{II} = Ni, Pd, Pt) layers with SCO properties sensitive to water inclusion.[10]

When Hofmann-like frameworks with pyridine and diazines are well studied and documented, there are three basic strategies to explore new ligands for building SCO cyanometalates. The first one consists in elongation of the interlayer space by incorporating bis- and polypyridyl ligands that in certain cases makes voids in the resulting MOFs accessible for bulky guest molecules.[11] Another approach is to use diazole and triazole ligands.[12] Finally, the SCO properties can be tuned successfully by introducing substituents into the aromatic ring of the axial ligands.[13] The transition temperature and bistable region appear to be influenced by the substituent type, size and involvement in interlayer interactions. We have shown previously that replacement of pyrazine by 2-methylpyrazine (Mepz) in $[Fe^{II}(Mepz)_2M^{II}(CN)_4]$ (M^{II} = Ni, Pd, Pt) shifts the transition temperatures for all three compounds towards lower temperatures.[14]

In this work, we exploit further Hofmann-like frameworks built up from Fe^{II}, Mepz and $[M^{I}(CN)_2]^-$ (M^{I} = Au, Ag) cyanometalates with a view to understand the impact upon the SCO parameters when using 2-substituted pyrazines as co-ligands. Starting with different bridging moieties, $[Au(CN)_2]^-$ and $[Ag(CN)_2]^-$, we obtained a $\{Fe^{II}(Mepz)[Au^{I}(CN)_2]_2\}$ framework with 3D structure and a 2D coordination polymer $\{Fe^{II}(Mepz)_2[Ag^{I}(CN)_2]_2\}$, abbreviated as **[Au]** and **[Ag]** throughout the text. The compound **[Au]** exhibits a two-stepped spin transition, while **[Ag]** remains HS during thermal cycling. We believe that weak interlayer interactions, Ag–π, Me–π and Ag–N are responsible for the cooperativity of the lattice and contribute to the different magnetic behavior of **[Au]** and **[Ag]**.

EXPERIMENTAL SECTION

Materials and General Procedures. Methylpyrazine, potassium dicyanoaurate, potassium dicyanoargentate and iron perchlorate hexahydrate were purchased from Alfa Aesar and used as received.

Synthesis. Powders of **[Au]** and **[Ag]** were obtained by mixing solutions of $Fe(ClO_4)_2 \cdot 6H_2O$ (0.1 mmol, 1 eq.) and Mepz (0.5 mmol, 5 eq.) in water (1 mL) with a solution of $K[Au(CN)_2]$ or $K[Ag(CN)_2]$ (0.2 mmol, 2 eq.) in water (1 ml). This yielded precipitates of **[Au]** (orange) or **[Ag]** (yellow), which were separated by centrifugation, washed with water, centrifuged, and dried in air. Elemental analysis for $C_9H_6N_6FeAu_2$: calcd. C, 16.68; H, 0.93; N, 12.97; found C, 16.78; H, 1.01; N, 12.91%; for $C_{14}H_{12}N_8FeAg_2$: calcd. C, 29.82; H, 2.14; N, 19.87; found C, 30.03; H, 2.19; N, 19.75%. Single crystals of **[Au]** and **[Ag]** were obtained by a slow diffusion method within three layers in a 10 mL test tube. One milliliter of aqueous solution containing either $K[Au(CN)_2]$ or $K[Ag(CN)_2]$ (0.2 mmol) was poured on the bottom of the tube. Then 2 mL of water-methanol (**[Au]**) or water-ethanol (**[Ag]**) mixture (1:1) were gently layered on the top. The third layer was a solution (1 mL) of $Fe(ClO_4)_2 \cdot 6H_2O$ (0.1 mmol) and Mepz (0.5 mmol) in the respective alcohol. In two weeks this yielded orange crystals in the second layer; they were collected and kept in the mother solution prior to the X-Ray diffraction experiments.

X-ray Diffraction. Single crystal X-ray data for **[Au]** was collected on an Oxford-Diffraction XCALIBUR E CCD diffractometer at 200 K and for **[Ag]** on a Bruker SMART diffractometer at 173 K, using Mo-Kα radiation in both cases. The structures were solved with the ShelXS using Direct Methods and refined with the ShelXL using Least Squares minimization.[15a] Olex2 was used as an interface to ShelX programs.[15b] Carbon atom of methyl groups in **[Au]** disordered between

8 positions were refined isotopically because of the low occupancy of 0.125. All other non-hydrogen atoms were refined using an anisotropic model. Hydrogen atoms of Mepz were placed at calculated positions and refined using a riding model. CCDC deposition numbers are 1986756 (for **[Ag]**) and 1986758 (for **[Au]**). Powder X-ray diffraction (PXRD) patterns were acquired on a Siemens D5000 diffractometer (λ = 1.5406 Å) over the 2Θ range of 10°−60°.

Magnetic susceptibility measurements. Temperature dependent magnetic susceptibility measurements were carried out using a Quantum Design MPMS-XL-5 SQUID magnetometer equipped with a 5 T magnet over the temperature range 5–360 K with a heating/cooling rate of 2 K min^{-1} and a magnetic field of 0.5 T. Diamagnetic corrections for the molecules were derived from the Pascal's constants. Fitting of the experimental data was performed using JulX software.

Mössbauer spectroscopy. ^{57}Fe Mössbauer spectra were recorded in transmission geometry using a constant acceleration Mössbauer spectrometer Wissel equipped with a liquid nitrogen gas-flow cryostat. ^{57}Co embedded in a rhodium matrix was used as Mössbauer source. Samples were prepared by placing the powders of **[Au]** or **[Ag]** (50 mg each) in PMMA sample holders. Fitting the experimental data was performed with the Recoil software. Hyperfine parameters uncertainties were evaluated from the covariance matrix of the fit. Isomer shifts are given relatively to α-Fe at room temperature.

RESULTS AND DISCUSSION

Crystal structure. The compound **[Au]** crystallizes in the tetragonal space group *I*4/*mmm* with two formula units per cell. A fragment of its structure, depicted in Figure 1a, shows the atom numbering scheme of the asymmetric unit. The asymmetric unit contains only one Fe atom, which is situated on an inversion center. It is coordinated by six nitrogen atoms in an approximately

regular octahedral environment FeN_6. The equatorial coordination sites of iron are occupied by four $[Au(CN)_2]^-$ units, while its axial positions are occupied by two Mepz molecules. The groups $[Au(CN)_2]^-$ are perfectly linear. The Fe1–N1–C1, N1–C1–Au1 and C1–Au–$C1^i$ angles are 180° as they lie on the special positions 4c (Au1), 2a (Fe1) and 8i (C1, N1) and propagate along the directions [100] and [010]. Each $[Au(CN)_2]^-$ anion bridges two iron cations forming infinite flat $\{Fe[Au(CN)_2]_2\}_\infty$ sheets that lie parallel to the [110] plane. The aromatic Mepz ring is disordered between two equivalent positions, and the methyl group of Mepz is disordered between eight positions. In the crystal structure taken at 200 K, the average Fe–N bond length, 2.02 Å, indicates that the iron atoms are in the mixed HS/LS state, a fact consistent with the results of magnetic susceptibility and Mössbauer spectroscopy measurements. In the parent compound $\{Fe(pyrazine)[Au(CN)_2]_2\}$, which exhibits a cooperative SCO, the average Fe–N bond lengths are 1.93 Å and 2.16 Å in the LS and HS states respectively. Using these values as reference, one can roughly estimate that in the crystal structure of **[Au]** at 200 K, ca. 60 % of iron centers are LS. However, this estimation is very approximate since the bond lengths can vary considerably from one cyanometalate to another.

Complex **[Au]** is closely related to $\{Fe(pyrazine)[Au(CN)_2]_2\}$, whose crystal structure was solved in the *Fmmm* space group.[16a] In both compounds, cyanoheterometallic sheets are pillared by diazine ligands, which bridge the iron atoms of the neighboring sheets, thereby generating a 3D framework (Figure 1b). Each network is interpenetrated by another identical net to minimize void space within the structure. The resulting interlayer distance is two times shorter than the distance between cyanoheterometallic sheets of the same net that makes internetwork aurophilic contacts Au···Au of 3.517(1) Å (*vs* 3.379-3.594 Å in $\{Fe(pyrazine)[Au(CN)_2]_2\}$ depending on the spin state) possible. The interpenetration of two nets in **[Au]** is shown in Figure 1c.

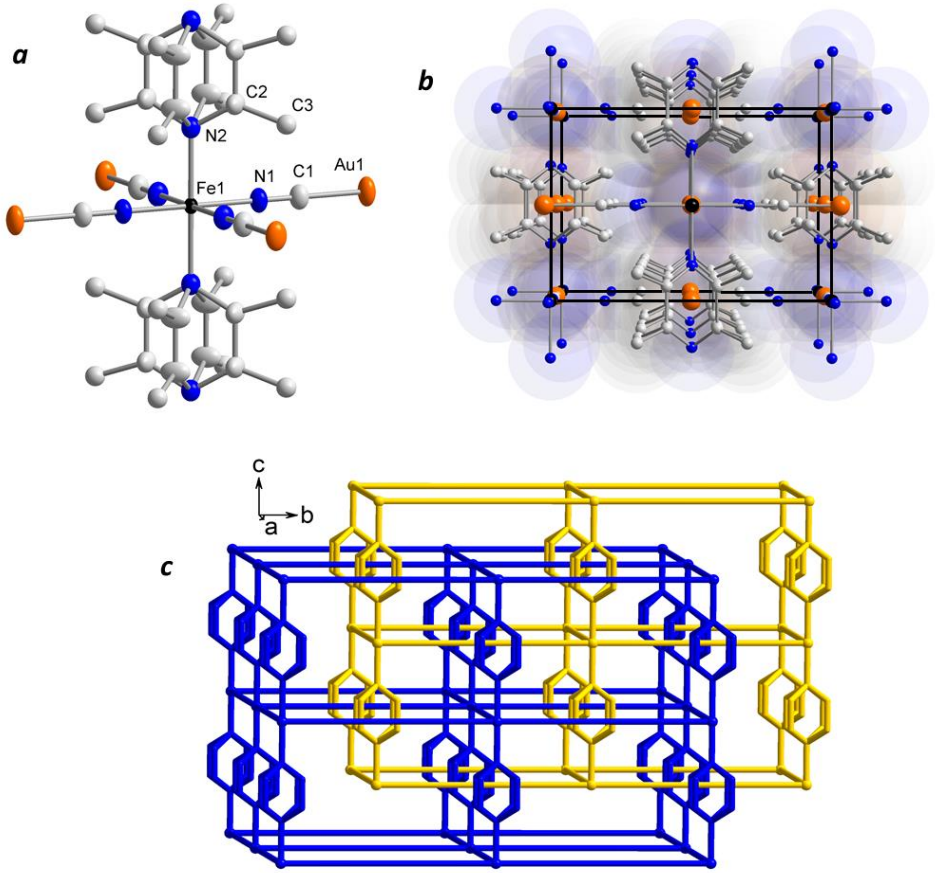

Figure 1. (a) Coordination environment of iron in **[Au]** with atomic displacement parameters shown at 50% probability. Only crystallographically unique atoms are labeled. Hydrogen atoms are omitted for clarity. (b) Fragment of the crystal structure showing the unit cell [Fe: black, Au: gold, N: blue, C: gray]. (c) View of the two identical interpenetrating nets in **[Au]** shown in blue and yellow.

Using $[Ag(CN)_2]^-$ as building block, one can expect to obtain the framework isostructural to **[Au]**. However, the topology of **[Ag]** obtained *via* an identical synthetic procedure is different. It crystallizes in the triclinic space group $P\bar{1}$ with one formula unit in the cell, where iron lies on the center of symmetry (Figure 2a). It resembles a FeN_6 unit typical for Hofmann-like frameworks,

built by axially coordinated Mepz ligands and four equatorially bound $[Ag(CN)_2]^-$ anions. In contrast to **[Au]**, Mepz ligands in **[Ag]** coordinate the iron sites *via* the nitrogen atom located distal to the methyl group, while the proximal nitrogen is not involved in the coordination. At 173 K, the average Fe–N bond lengths is 2.19 Å, characteristic of the HS iron(II), and the octahedral distortion parameter (the sum of the deviations from 90° for all 12 *cis* bond angles), Σ = 14.52°. The Ag–C≡N–Fe linkages are also distorted: the average Ag–C–N and C–N–Fe angles are 174.28° and 168.58° respectively, while angles C–Ag–C remain 180°, as silver atoms are located on special positions 1b and 1c, while bound by symmetry related carbon atoms. Differently from **[Au]**, but similarly to the complexes built from $[M(CN)_4]^{2-}$ (M = Ni, Pd, Pt) units and 2-substituted pyridines,[13a] the cyanoheterometallic sheets in **[Ag]** are corrugated (Figure 2b), as nitrogen atoms lie 0.366 Å above and below the plane defined by silver atoms.

While **[Au]**, {Fe(pyrazine)$[Au(CN)_2]_2$},[16a] and its silver analogue {Fe(pyrazine)$[Ag(CN)_2]_2$},[16b] form very similar 3D networks with SCO, cyanoheterometallic layers in **[Ag]** are not bridged by the diazine ligand (Figure 2c). Instead they are held together by a combination of weak interactions, which allow us to consider **[Ag]** only as a pseudo-3D framework. Specifically, every other silver atom, Ag1, is situated between two Mepz rings, which belong to the neighboring cyanoheterometallic layers. The length of these Ag–π contacts is 3.287(1) Å, and the acute angle C1–Ag1–π is 84.21°. From another side of the aromatic ring, every Mepz ligand forms a Me–π contact with a methyl group of another Mepz ligand, which coordinates two iron layers above or below (Figure 2d). Because the H atoms of methyl groups are placed at the calculated positions in the crystal structure, the length of the Me–π contacts can be estimated as the distance from the carbon atom of the methyl group to the center of the aromatic ring. It is 3.441(2) Å, notably shorter than the reference value of 3.7 Å,[17] and the acute angle C4–C7–π is 90.81°. All in all, combination

of the alternating pairs of Ag–π and Me–π contacts form infinite rows of weak interactions parallel to the cyanoheterometallic sheets and they involve three of these sheets. In addition, the cyanoheterometallic layers are stitched together through the Ag2–N4 contacts of 3.349(1) Å between every other silver atom and the nitrogen atoms not involved in coordination of iron. As the structures of the two title frameworks are different, Ag···Ag contacts are not present in **[Ag]**. Selected bond distances and angles for **[Ag]** and **[Au]** are compared in the Table 1.

Magnetic properties. Temperature-dependent magnetic susceptibility measurements for **[Au]** were conducted to follow the iron(II) spin-state changes (Figure 3). The product of the molar magnetic susceptibility with temperature, $\chi_M T$, as a function of temperature reveals an incomplete stepped SCO for this compound. At 360 K, $\chi_M T$ is 3.3 $cm^3\,K\,mol^{-1}$, indicative of all iron(II) sites existing in the HS state. Upon cooling, a decrease of $\chi_M T$ to 2.3 $cm^3\,K\,mol^{-1}$ over the temperature range 340 – 285 K was observed. Further cooling reveals a more gradual decrease in $\chi_M T$, reaching 1.2 $cm^3\,K\,mol^{-1}$ at 80 K. This behavior can be interpreted as a two-step HS to LS transition in ca. 70% of the SCO centers. Below 80 K, $\chi_M T$ remains approximately constant until an abrupt drop below 30 K due to zero-field splitting (ZFS) appears which is caused by residual HS iron(II) sites.

The incomplete stepped SCO behavior in **[Au]** can be explained by the existence of three Fe types in the compound with different SCO temperatures. Specifically, Fe atoms can be coordinated by 1N and 1N (25%), or 1N and 4N (50%), or 4N and 4N (25%) atoms of two axial Mepz ligands. As Mepz molecules are disordered in the crystal structure of **[Au]**, these Fe types are crystallographically identical. Therefore, the observed SCO steps cannot be confidently assigned to specific Fe types. It is, however, clear that one of the Fe types with 25% population remains HS in the whole temperature range, while two other types undergo spin transition with T_{SCO} = 170 K and 308 K. We assume that the more gradual transition with T_{SCO} = 170 K corresponds to the Fe

centers coordinated by 1N and 4N atoms of Mepz (50% of all centers), and this step is incomplete on cooling, as part of these Fe centers remain trapped in the HS state below 80 K. In contrast, a similar Hofmann-like framework {Fe(2-fluoropyrazine)[Au(CN)$_2$]$_2$} reported by Real *et al.* exhibits a complete one-step SCO with a wide hysteresis loop.[13e] The difference between the two complexes can be explained by the dynamic disorder of Mepz in **[Au]**, which contributes to the higher flexibility of the structure.

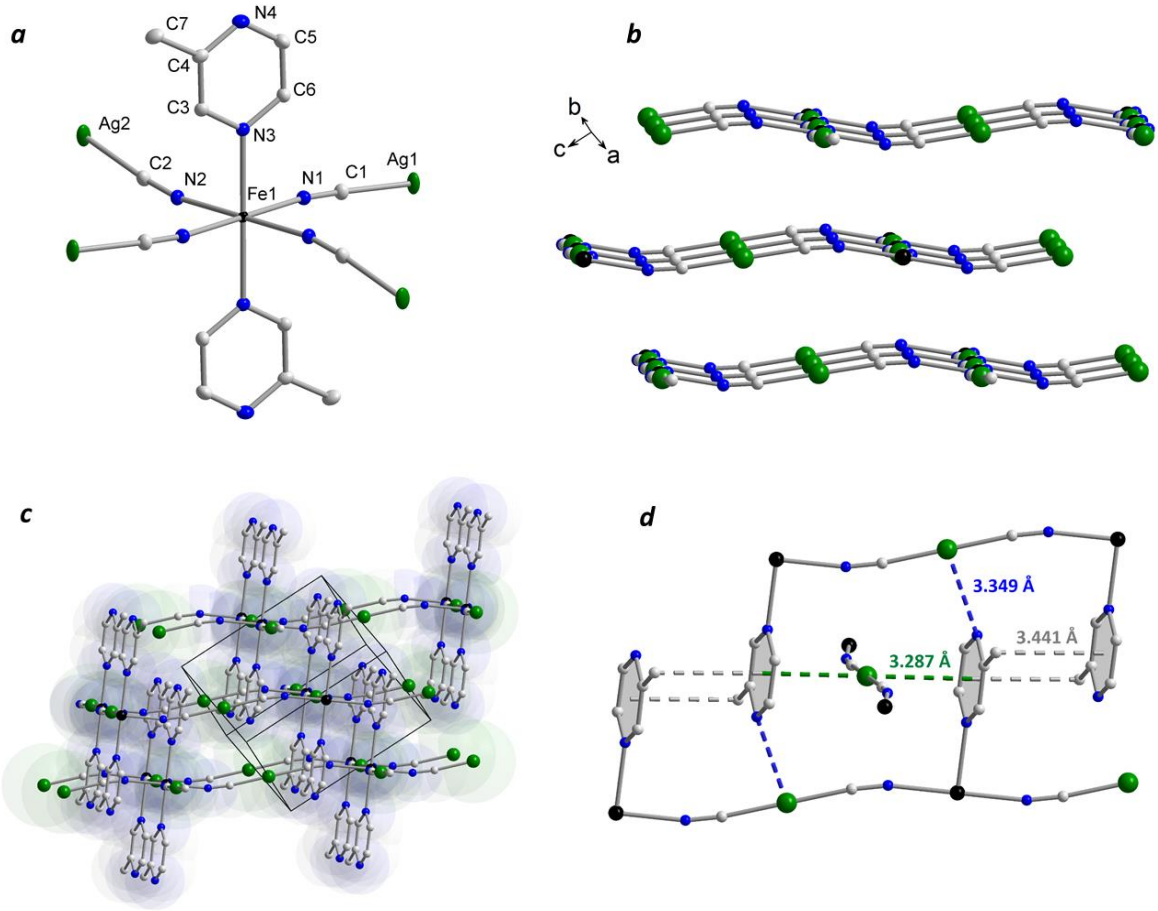

Figure 2. (a) Fragment of the crystal structure of **[Ag]** showing coordination environment of iron with atomic displacement parameters depicted at 50% probability. Hydrogen atoms are omitted for clarity. (b) View of the corrugated cyanoheterometallic layers shown in blue. Mepz ligands are

shown in gray. (c) Unit cell. (d) Short interlayer Ag–π and Me–π contacts shown as dashed green and gray lines respectively [Fe: black, Ag: green, N: blue, C: gray].

Table 1. Selected bond distances [Å] and angles [deg] of **[Au]** (200 K) and **[Ag]** (173 K)

	[Au]	**[Ag]**
	distances [a]	
<Fe–N_{CN}>	2.09(2)	2.159(2)
<Fe–N_{pz}>	1.98(2)	2.250(1)
<M–C_{CN}>	1.971(1)	2.070(3)
	angles [b]	
N_{CN}–Fe–N^{i}_{CN}	90	88.54(5)
N_{pz}–Fe–N_{CN}	90	89.57(5)
N_{pz}–Fe–N^{i}_{CN}	90	88.33(5)

[a] chevrons denote average distances; [b] only acute angles are given

With heating of the sample in the magnetic field, its susceptibility behavior is completely reversible, with only a narrow hysteresis observed during the $HS_{0.67}LS_{0.33}$→HS transition. From the $\chi_M T$ *vs* T behavior the following SCO parameters can be extracted: T_{SCO1} = 170 K, T_{SCO2}^{up} = 310 K and T_{SCO2}^{down} = 306 K, where SCO1 and SCO2 stand for the $HS_{0.33}LS_{0.67}$→$HS_{0.67}LS_{0.33}$ and the $HS_{0.67}LS_{0.33}$→HS transitions. During the subsequent cycle of cooling from 360 K to 60 K and warming from 60 K to 360 K, these parameters remain unchanged. The first and second thermal cycles are virtually identical, most likely because the framework of **[Au]** does not contain any guest molecules and is thermally stable within the operated temperature region.

The gradual transitions at both steps and narrow irregular shape hysteresis indicate weak cooperativity between the SCO centers compared to the related {Fe(pyrazine)[Au(CN)$_2$]$_2$} with one-step abrupt — and complete — transition above room temperature. Notably, introduction of substituents to the pyrazine ring is associated with multistep spin transitions in the family of Hofmann-like clathrates.[13d-e,14] Previously we have shown that [Fe(2-chloropyrazine)$_2$Ni(CN)$_4$] and [Fe(2-methylpyrazine)$_2$Ni(CN)$_4$] display a two-step transition versus a one-step transition in [Fe(pyrazine)Ni(CN)$_4$], for all three complexes below room temperature.[14] Remarkably, the intermediate state HS$_{0.67}$LS$_{0.33}$ is stabilized for **[Au]** around ambient temperature. Due to a pronounced thermochromism, the orange powder of as-synthesized **[Au]** turns scarlet upon cooling to 78 K and yellow when heated above room temperature. Magnetic susceptibility measurements reveal that **[Ag]** is HS at room temperature and remains HS on cooling. It exhibits a typical for HS iron(II) Curie-type behavior with $\chi_M T$ = 3.26 cm^3 K mol^{-1}.

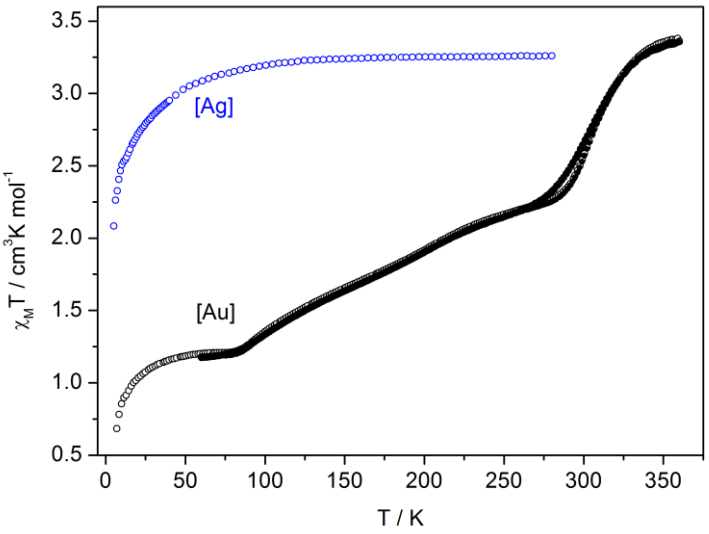

Figure 3. Magnetic properties of **[Au]** and **[Ag]** in the form of $\chi_M T$ *vs* T. For **[Au]**, two consecutive thermal cycles are shown (open circles: first cycle, filled circles: second cycle).

Comparing the two title complexes with regard to their structure and magnetic properties, we note that the coordination polyhedron in **[Ag]** is unusually elongated. The axial coordination bonds Fe1–N3 are 2.250(1) Å, considerably higher than for the HS forms of other Hofmann-type frameworks containing bridging or terminal aromatic N-donor ligands (Figure S2).[8,10-14] This large elongation cannot be explained solely by the Jahn-Teller effect of the ^5T manifold. In the crystal structure of **[Ag]**, the Mepz ligands are involved in the net of intermolecular interactions Ag–π, Me–π and Ag–N in the most efficient manner, *i.e.* silver atoms and methyl groups are located perfectly above (or below) the aromatic ring, which determines more distant position of the Mepz ligand from the iron center. As a result, the iron ions are trapped in their HS state, because the need to maintain the 3D framework *via* intermolecular interactions prevents a contraction of the iron coordination sphere.[4] In other words, the expected LS form of **[Ag]** differs too strongly from its actual HS form, and the structural change associated with SCO is too great to be accommodated by the framework. The similar effect was observed in a few other families of SCO complexes, allowing to conclude that the high packing density in a structure with numerous short intermolecular contacts responsible for cooperativity can inhibit the structural transition accompanying SCO.[5] In particular, Reger *et al.* made an argument that a more organized 3D supramolecular structure would disfavor SCO for this reason.[18]

^{57}Fe Mössbauer spectroscopy. Application of Mössbauer spectroscopy to investigate the origin of the stepped spin transition in **[Au]** was challenging because of the presence of two gold atoms with high non-resonant γ-ray absorbance per one iron atom in the formula unit. At room temperature the spectrum shows two symmetric doublets with relative intensities of 57% and 43% suggesting the coexistence of two spin forms of iron (Figure 4). For one of the doublets, the isomer shift $\delta = 0.81(1)$ mm s^{-1} and quadrupole splitting $|\Delta E_Q| = 1.17(2)$ mm s^{-1}, are consistent with values

expected for iron(II) in the HS state. For a minor doublet, $\delta = 0.52(1)$ mm s^{-1} and $|\Delta E_Q| = 0.16(2)$ mm s^{-1} are representative of the LS iron. The isomer shift of the LS iron in **[Au]** is comparably higher than that in {Fe(pyrazine)[Au(CN)$_2$]$_2$} ($\delta = 0.35$ mm s^{-1} at 293 K),[16a] most likely due to the higher *d*-electron density at iron atoms coordinated by Mepz. To the best of our knowledge, there are no other gold-containing Hofmann-like cyanometalates with reported Mössbauer spectra for comparison.

When **[Au]** is cooled to 80 K, the relative intensity of the HS doublet decreases to 34%, and intensity for the LS doublet increases to 66% due to the gradual step of spin transition between room temperature and 80 K. It should be mentioned that relative intensities of the high-spin doublet are expected to be underestimated (especially at room temperature) due to the lower Debye-Waller factor compared to the LS iron.[19] The isomer shift $\delta = 1.08(2)$ mm s^{-1} for the HS doublet at 80 K is higher than at 293 K due to the second-order Doppler shift, while the position of the LS doublet ($\delta = 0.52(2)$ mm s^{-1} at 80 K) is not affected. In addition, for the HS doublet $|\Delta E_Q|$ is ca. 0.4 mm s^{-1} larger at 80 K than at 293 K because of the larger difference in the population of the d_{xy} and d_{xz}/d_{yz} levels at lower temperatures. Accordingly, $|\Delta E_Q|$ for the LS doublet remains unchanged because the orbitals d_{xy}, d_{xz} and d_{yz} are fully occupied, independent of the temperature.

In the Mössbauer spectra of **[Ag]** recorded at 293 K and 80 K, a single quadrupole doublet corresponding to the HS state of iron(II) was found. This is consistent with the results of the magnetic susceptibility measurements. The hyperfine parameters of the doublet (293 K: $\delta = 1.09(1)$ mm s^{-1}, $|\Delta E_Q| = 1.17(2)$ mm s^{-1}; 80 K: $\delta = 1.20(1)$ mm s^{-1}, $|\Delta E_Q| = 1.81(2)$ mm s^{-1}) are comparable to those reported for the related compounds {Fe(L)$_x$[Ag(CN)$_2$]$_2$} (L = 4,4′-bis(pyridyl)acetylene, 3-methylpyridine, 4-methylpyridine, 3,4-dimethylpyridine and 3-

chloropyridine).[11a,13d] The Mössbauer parameters for **[Au]** and **[Ag]** are summarized in the Table 2.

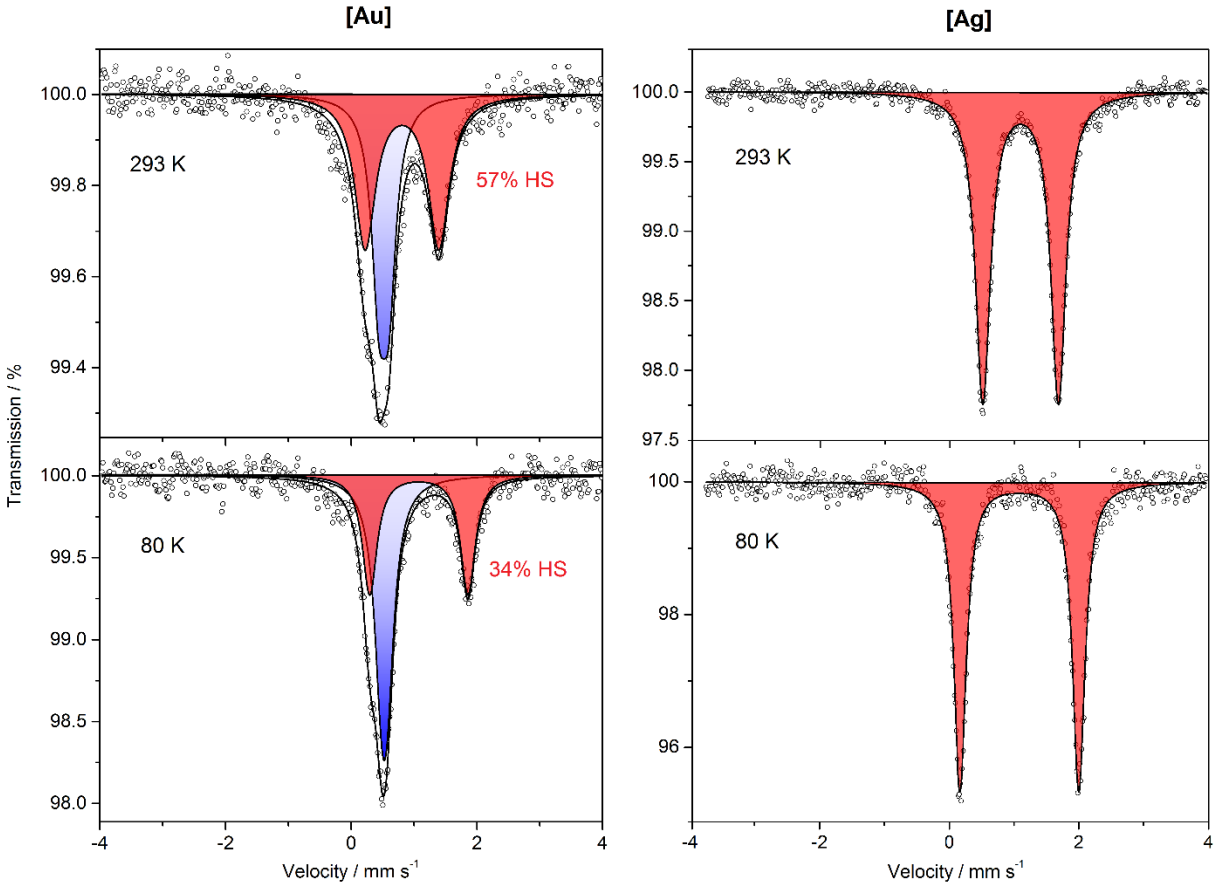

Figure 4. Mössbauer spectra of **[Au]** and **[Ag]** recorded at 293 K and 80 K showing LS and HS iron(II) doublets in blue and red, respectively.

Table 2. Hyperfine parameters [mm s^{-1}] for **[Au]** and **[Ag]** derived from their Mössbauer spectra

T	Parameter	**[Au]**		**[Ag]**
		LS	HS	HS
293 K	δ	0.52(1)	0.81(1)	1.09(1)
	$\|\Delta E_Q\|$	0.16(2)	1.17(2)	1.17(2)

	content	43%	57%	100%
80 K	δ	0.52(2)	1.08(2)	1.20(1)
	$\|\Delta E_Q\|$	0.09(7)	1.56(6)	1.81(2)
	content	66%	34%	100%

CONCLUSIONS

Starting from Fe^{II}, Mepz and $[M(CN)_2]^-$ (M = Au, Ag), two Hofmann-type coordination polymers, **[Au]** and **[Ag]**, were obtained. Despite of the very similar building blocks, the structures of the two compounds are very different. The complex **[Au]** has the same structural features as its parent compounds {Fe(pyrazine)$[M(CN)_2]_2$} (M = Au, Ag). This allows a direct comparison between their properties. It shows a two-step thermal SCO that is incomplete at low temperatures. The stepped character of the spin transition can be explained by the existence of three types of Fe atoms, based on the coordination manner of the axial Mepz ligands. Replacement of the pyrazine ligand by Mepz leads to a loss of cooperativity most likely due to the mobility of Mepz in the crystal structure. This makes **[Au]** differrent from {Fe(pyrazine)$[Au(CN)_2]_2$}, whose rigid lattice leads to the cooperative SCO accompanied by a colossal anisotropic structural distortion.[16a]

The complex **[Ag]** crystallizes with two Mepz molecules per Fe^{II}, because Mepz does not bridge Fe^{II} atoms. Nonetheless, the corrugated cyanoheterometallic sheets are connected *via* the network of Ag–π, Me–π and Ag–N interactions. It forces the axial Fe–N_{Mepz} bonds to be unusually elongated. Upon cooling, **[Ag]** remains HS, as a transition to the LS state would require dramatic changes to the frameworks due to the contraction of the coordinative bonds. All in all, this is a prototypical example showing that the ability of a lattice to accommodate structural changes associated with a spin transition plays an important role in determining the existence of a SCO in

the solid state.[4,5] In the present case, the use of either precious metal for synthesis defines the properties of the material.

This study also demonstrates that SCO characteristics in the family of Hofmann-type cyanometalates can easily be tuned by introducing substituents into the pyrazine ring. The versatility of substituted pyrazines provides one avenue to explore further this immense class of SCO complexes.

ASSOCIATED CONTENT

Supporting Information. The following files are available free of charge.

Supplementary figures (S1-S2) and crystallographic tables (PDF)

X-ray crystallographic data for **[Au]** (CIF)

X-ray crystallographic data for **[Ag]** (CIF)

AUTHOR INFORMATION

Corresponding Author

* Il'ya A. Gural'skiy. E-mail: illia.guralskyi@univ.kiev.ua

Author Contributions

The manuscript was written through contributions of all authors. All authors have given approval to the final version of the manuscript.

Funding Sources

European Commission (Horizon 2020 MSCA-RISE-2016 grant No. 73422); Ministry of Education and Science of Ukraine (Fundamental research grant No. 19BF037-01M).

Notes

The authors declare no competing financial interest.

ACKNOWLEDGMENT

This work was supported by the Horizon 2020 MSCA-RISE-2016 grant (project No. 73422) and 19BF037-01M grant obtained from the Ministry of Education and Science of Ukraine. SIS thanks the ÅForsk Foundation for support.

REFERENCES

(1) Gütlich, P.; Goodwin, H. Spin Crossover – An Overall Perspective. *Topics in Current Chemistry* **2004**, *233*, 1–47.

(2) For selected reviews on spin crossover in Fe(II) complexes, see: (a) Gaspar, A. B.; Ksenofontov, V.; Seredyuk, M.; Gütlich, P. Multifunctionality in spin crossover materials. *Coord. Chem. Rev.* **2005**, *249*, 2661–2676. (b) Gütlich, P.; Gaspar, A. B.; Garcia, Y. Spin state switching in iron coordination compounds. *Beilstein J. Org. Chem.* **2013**, *9*, 342–391. (c) Bousseksou, A.; Molnar, G.; Salmon, L.; Nicolazzi, W. Molecular spin crossover phenomenon: recent achievements and prospects. *Chem. Soc. Rev.* **2011**, *40*, 3313–3335. (d) Hogue, R. W.; Singh, S.; Brooker, S. Spin crossover in discrete polynuclear iron(II) complexes. *Chem. Soc. Rev.* **2018**, *47*, 7303–7338. (e) Kumar, K. S.; Ruben, M. Emerging trends in spin crossover (SCO) based functional materials and devices. *Coord. Chem. Rev.* **2017**, *346*, 176–205. (f) Collet, E.; Guionneau, P. Structural analysis of spin-crossover materials: From molecules to materials. *C. R. Chim.* **2018**, *21*, 1133–1151. (g) Gaspar, A. B.; Molnár, G.; Rotaru, A.; Shepherd, H. J. Pressure effect investigations on spin-crossover

coordination compounds. *C. R. Chim.* **2018**, *21*, 1095–1120. (h) Boillot, M.-L.; Weber, B. Mononuclear ferrous and ferric complexes. *C. R. Chim.* **2018**, *21*, 1196–1208.

(3) (a) Murray, K. S.; Kepert, C. J. Cooperativity in Spin Crossover Systems: Memory, Magnetism and Microporosity. *Topics in Current Chemistry* **2004**, *233*, 195–228. (b) Halcrow, M. A. Spin-crossover Compounds with Wide Thermal Hysteresis. *Chem. Lett.* **2014**, *43*, 1178–1188. (c) Brooker, S. Spin crossover with thermal hysteresis: practicalities and lessons learnt. *Chem. Soc. Rev.* **2015**, *44*, 2880–2892.

(4) Halcrow, M. A. Structure:function relationships in molecular spin-crossover complexes. *Chem. Soc. Rev.* **2011**, *40*, 4119–4142.

(5) (a) Elhaïk, J.; Kilner, C. A.; Halcrow, M. A. Structural diversity in iron(II) complexes of 2,6-di(pyrazol-1-yl)pyridine and 2,6-di(3-methylpyrazol-1-yl)pyridine. *Dalton Trans.* **2006**, 823–830. (b) Reger, D. L.; Little, C. A.; Smith, M. D.; Rheingold, A. L.; Lam, K.-C.; Concolino, T. L.; Long, G. J.; Hermann, R. P.; Grandjean, F. Synthetic, Structural, Magnetic, and Mössbauer Spectral Study of $\{Fe[HC(3,5\text{-}Me_2pz)_3]_2\}I_2$ and its Spin-State Crossover Behavior. *Eur. J. Inorg. Chem.* **2002**, 1190–1197. (c) Bauer, W.; Weber, B. X-ray structure and magnetic properties of dinuclear and polymer iron(II) complexes. *Inorg. Chim. Acta* **2009**, *362*, 2341–2346. (d) Sheu, C. F.; Pillet, S.; Lin, Y. C.; Chen, S. M.; Hsu, I. J.; Lecomte, C.; Wang, Y. Magnetostructural Relationship in the Spin-Crossover Complex t-$\{Fe(abpt)_2[N(CN)_2]_2\}$: Polymorphism and Disorder Phenomenon. *Inorg. Chem.* **2008**, *47*, 10866–10874. (e) Ozarowski, A.; McGarvey, B. R.; Sarkar, A. B.; Drake, J. E. EPR study of manganese(II) in two crystalline forms of bis(2,2'-bi-2-thiazoline)bis(thiocyanato)iron and the high-spin-low-spin transition that occurs in only one form. X-ray structure determination of

both forms. *Inorg. Chem.* **1988**, *27*, 628–635. (f) Matouzenko, G. S.; Bousseksou, A.; Lecocq, S.; van Koningsbruggen, P. J.; Perrin, M.; Kahn, O.; Collet, A. Polymorphism in Spin Transition Systems. Crystal Structure, Magnetic Properties, and Mössbauer Spectroscopy of Three Polymorphic Modifications of [Fe(DPPA)$(NCS)_2$] [DPPA = (3-Aminopropyl)bis(2-pyridylmethyl)amine]. *Inorg. Chem.* **1997**, *36*, 5869–5879. (g) Hang, H.; Fei, B.; Chen, X. Q.; Tong, M. L.; Ksenofontov, V.; Gural'skiy, I. A.; Bao, X. Multiple spin phases in a switchable Fe(II) complex: polymorphism and symmetry breaking effects. *J. Mater. Chem. C* **2018**, *6*, 3352–3361.

(6) (a) Muñoz, M. C.; Real, J. A. Thermo-, piezo-, photo- and chemo-switchable spin crossover iron(II)-metallocyanate based coordination polymers. *Coord. Chem. Rev.* **2011**, *255*, 2068–2093. (b) Polyzou, C. D.; Tangoulis, V. Review. Downsizing Effect on 2-D and 3-D Spin Crossover Metal-Organic Frameworks. *J. Coord. Chem.* **2019**, 72 , 389–418. (c) Ohtani, R.; Hayami, S. Guest-Dependent Spin-Transition Behavior of Porous Coordination Polymers. *Chem. - A Eur. J.* **2017**, 23, 2236–2248. (d) Ni, Z.-P.; Liu, J.-L.; Hoque, M. N.; Liu, W.; Li, J.-Y.; Chen, Y.-C.; Tong, M.-L. Recent Advances in Guest Effects on Spin-Crossover Behavior in Hofmann-Type Metal-Organic Frameworks. *Coord. Chem. Rev.* **2017**, 335, 28–43.

(7) Kitazawa, T.; Gomi, Y.; Takahashi, M.; Takeda, M.; Enomoto, M.; Miyazaki, A.; Enoki, T. Spin-crossover behaviour of the coordination polymer $Fe^{II}(C_5H_5N)_2Ni^{II}(CN)_4$. *J. Mater. Chem.* **1996**, *6*, 119–121.

(8) (a) Niel, V.; Martinez-Agudo, J. M.; Muñoz, M. C.; Gaspar, A. B.; Real, J. A. Cooperative Spin Crossover Behavior in Cyanide-Bridged Fe(II)−M(II) Bimetallic 3D Hofmann-like

Networks (M = Ni, Pd, and Pt). *Inorg. Chem.* **2001**, *40*, 3838–3839. (b) Agustí, G.; Ohtani, R.; Yoneda, K.; Gaspar, A. B.; Ohba, M.; Sánchez-Royo, J. F.; Muñoz, M. C.; Kitagawa, S.; Real, J. A. Oxidative Addition of Halogens on Open Metal Sites in a Microporous Spin-Crossover Coordination Polymer. *Angew. Chem., Int. Ed.* **2009**, *48*, 8944–8947. (c) Niel, V.; Thompson, A. L.; Muñoz, M. C.; Galet, A.; Goeta, A. E.; Real, J. A. Crystalline-state reaction with allosteric effect in spin-crossover, interpenetrated networks with magnetic and optical bistability. *Angew. Chem., Int. Ed.* **2003**, *42*, 3760–3763. (d) Niel, V.; Galet, A.; Gaspar, A. B.; Muñoz, M. C.; Real, J. A. Cooperative thermal and optical switching of spin states in a new two-dimensional coordination polymer. *Chem. Commun.* **2003**, 1248–1249. (e) Rodriguez-Velamazan, J. A.; Canadillas-Delgado, L.; Castro, M.; McIntyre, G. J.; Real, J. A. Temperature- and pressure-dependent structural study of $\{Fe(pmd)_2[Ag(CN)_2]_2\}_n$ spin-crossover compound by neutron Laue diffraction. *Acta Cryst. B* **2014**, *70*, 436–443. (f) Galet, A.; Muñoz, M. C.; Gaspar, A. B.; Real, J. A. Architectural Isomerism in the Three-Dimensional Polymeric Spin Crossover System $\{Fe(pmd)_2[Ag(CN)_2]_2\}$: Synthesis, Structure, Magnetic Properties, and Calorimetric Studies. *Inorg. Chem.* **2005**, *44*, 8749–8755.

(9) (a) Levchenko, G.; Gaspar, A. B.; Bukin, G.; Berezhnaya, L.; Real, J. A. Pressure Effect Studies on the Spin Transition of Microporous 3D Polymer $[Fe(pz)Pt(CN)_4]$. *Inorg. Chem.* **2018**, *57*, 8458-8464. (b) Pham, C. H.; Paesani, F. Spin Crossover in the $\{Fe(pz)[Pt(CN)_4]\}$ Metal–Organic Framework upon Pyrazine Adsorption. *J. Phys. Chem. Lett.* **2016**, *7*, 4022–4026. (c) Raza, Y.; Volatron, F.; Moldovan, S.; Ersen, O.; Huc, V.; Martini, C.; Brisset, F.; Gloter, A.; Stephan, O.; Bousseksou, A.; Catala, L.; Mallah, T. Matrix-dependent cooperativity in spin crossover $Fe(pyrazine)Pt(CN)_4$ nanoparticles. *Chem. Commun.* **2011**, *47*, 11501–11503. (d) Delgado, T.; Enachescu, C.; Tissot, A.; Guénée, L.; Hauser, A.; Besnard,

C. The influence of the sample dispersion on a solid surface in the thermal spin transition of [Fe(pz)Pt(CN)$_4$] nanoparticles. *Phys. Chem. Chem. Phys.* **2018**, *20*, 12493–12502. (e) Bartual-Murgui, C.; Salmon, L.; Akou, A.; Thibault, C.; Molnár, G.; Mahfoud, T.; Sekkat, Z.; Real, J. A.; Bousseksou, A. High quality nano-patterned thin films of the coordination compound {Fe(pyrazine)[Pt(CN)$_4$]} deposited layer-by-layer. *New J. Chem.* **2011**, *35*, 2089–2094.

(10) Gural'skiy, I. A.; Shylin, S. I.; Ksenofontov, V.; Tremel, W. Pyridazine-Supported Polymeric Cyanometallates with Spin Transitions. *Eur. J. Inorg. Chem.* **2019**, 4532–4537.

(11) (a) Shepherd, H. J.; Bartual-Murgui, C.; Molnár, G.; Real, J. A.; Muñoz, M. C.; Salmon, L.; Bousseksou, A. Thermal and pressure-induced spin crossover in a novel three-dimensional Hoffman-like clathrate complex. *New J. Chem.* **2011**, *35*, 1205–1210. (b) Sciortino, N. F.; Scherl-Gruenwald, K. R.; Chastanet, G.; Halder, G. J.; Chapman, K. W.; Létard, J.-F.; Kepert, C. J. Hysteretic three-step spin crossover in a thermo- and photochromic 3D pillared Hofmann-type metal-organic framework. *Angew. Chem., Int. Ed.* **2012**, *51*, 10154–10158. (c) Agustí, G.; Cobo, S.; Gaspar, A. B.; Molnár, G.; Moussa, N. O.; Szilágyi, P. Á.; Pálfi, V.; Vieu, C.; Carmen Muñoz, M.; Real, J. A.; Bousseksou, A. Thermal and Light-Induced Spin Crossover Phenomena in New 3D Hofmann-Like Microporous Metalorganic Frameworks Produced as Bulk Materials and Nanopatterned Thin Films. *Chem. Mater.* **2008**, *20*, 6721–6732. (d) Muñoz-Lara, F. J.; Gaspar, A. B.; Muñoz, M. C.; Arai, M.; Kitagawa, S.; Ohba, M.; Real, J. A. Sequestering Aromatic Molecules with a Spin-Crossover Fe^{II} Microporous Coordination Polymer. *Chem. - Eur. J.* **2012**, *18*, 8013–8018. (e) Li, J.-Y.; He, C.-T.; Chen, Y.-C.; Zhang, Z.-M.; Liu, W.; Ni, Z.-P.; Tong, M.-L. Tunable cooperativity in a spin-crossover Hoffman-like metal–organic framework material by aromatic guests. *J. Mater. Chem. C* **2015**, *3*, 7830–7835. (f) Kosone, T.; Kitazawa, T. Guest-dependent spin transition

with long range intermediate state for 2-dimensional Hofmann-like coordination polymer. *Inorg. Chim. Acta* **2016**, *439*, 159–163. (g) Hiiuk, V. M.; Shova, S.; Rotaru, A.; Ksenofontov, V.; Fritsky, I. O.; Gural'skiy, I. A. Room temperature hysteretic spin crossover in a new cyanoheterometallic framework. *Chem. Commun.* **2019**, *55*, 3359–3362. (h) Zhang, C.-J.; Lian, K.-T.; Huang, G.-Z.; Bala, S.; Ni, Z.-P.; Tong, M.-L. Hysteretic four-step spin-crossover in a 3D Hofmann-type metal–organic framework with aromatic guest. *Chem. Commun.*, **2019**, *55*, 11033–11036. (i) Murphy, M. J.; Zenere, K. A.; Ragon, F.; Southon, P. D.; Kepert, C. J.; Neville, S. M. Guest Programmable Multistep Spin Crossover in a Porous 2-D Hofmann-Type Material. *J. Am. Chem. Soc.* **2017**, 139, 1330−1335. (j) Zhang, C.-J.; Lian, K.-T.; Huang, G.-Z.; Bala, S.; Ni, Z.-P.; Tong, M.-L. Hysteretic Four-Step Spin-Crossover in a 3D Hofmann-Type Metal–Organic Framework with Aromatic Guest. *Chem. Commun.* **2019**, 55, 11033–11036.

(12) (a) Munoz-Lara, F. J.; Gaspar, A. B.; Munoz, M. C.; Lysenko, A. B.; Domasevitch, K. V.; Real, J. A. Fast detection of water and organic molecules by a change of color in an iron(II) microporous spin-crossover coordination polymer. *Inorg. Chem.* **2012**, *51*, 13078–13080. (b) Sciortino, N. F.; Zenere, K. A.; Corrigan, M. E.; Halder, G. J.; Chastanet, G.; Létard, J.-F.; Kepert, C. J.; Neville, S. M. Four-step iron(II) spin state cascade driven by antagonistic solid state interactions. *Chem. Sci.* **2017**, *8*, 701–707.

(13) (a) Martínez, V.; Gaspar, A. B.; Muñoz, M. C.; Bukin, G. V.; Levchenko, G.; Real, J. A. Synthesis and Characterisation of a New Series of Bistable Iron(II) Spin-Crossover 2D Metal–Organic Frameworks. *Chem. - Eur. J.* **2009**, *15*, 10960–10971. (b) Liu, W.; Wang, L.; Su, Y.-J.; Chen, Y.-C.; Tucek, J.; Zboril, R.; Ni, Z.-P.; Tong, M.-L. Hysteretic Spin Crossover in Two-Dimensional (2D) Hofmann-Type Coordination Polymers. *Inorg. Chem.* **2015**, *54*,

8711–8716. (c) Agustí, G.; Gaspar, A. B.; Muñoz, M. C.; Real, J. A. Thermal- and Pressure-Induced Cooperative Spin Transition in the 2D and 3D Coordination Polymers {Fe(5-Br-pmd)$_z$[M(CN)$_x$]$_y$} (M = Ag^I, Au^I, Ni^{II}, Pd^{II}, Pt^{II}). *Inorg. Chem.* **2007**, *46*, 9646–9654. (d) Rodríguez-Velamazán, J. A.; Carbonera, C.; Castro, M.; Palacios, E.; Kitazawa, T.; Létard, J.-F.; Burriel, R. Two-Step Thermal Spin Transition and LIESST Relaxation of the Polymeric Spin-Crossover Compounds Fe(X-py)$_2$[Ag(CN)$_2$]$_2$ (X=H, 3-methyl, 4-methyl, 3,4-dimethyl, 3-Cl). *Chem. - Eur. J.* **2010**, *16*, 8785–8796. (e) Valverde-Muñoz, F. J.; Seredyuk, M.; Muñoz, M. C.; Znovjyak, K.; Fritsky, I. O.; Real, J. A. Strong Cooperative Spin Crossover in 2D and 3D Fe^{II}–M^{I,II} Hofmann-Like Coordination Polymers Based on 2-Fluoropyrazine. *Inorg. Chem.* **2016**, *55*, 10654–10665. (f) Polyzou, C. D.; Malina, O.; Tuček, J.; Zbořil, R.; Panagiotou, N.; Tasiopoulos, A. J.; Boukos N.; Parthenios, J.; Kalarakis, A. N.; Tangoulis, V. Spin-Crossover Phenomenon in Microcrystals and Nanoparticles of a [Fe(2-mpz)$_2$Ni(CN)$_4$] Two-Dimensional Hofmann-Type Polymer: A Detailed Nano-Topographic Study. *Inorg. Chem.* **2019**, *58*, 13733–13736.

(14) Kucheriv, O. I.; Shylin, S. I.; Ksenofontov, V.; Dechert, S.; Haukka, M.; Fritsky, I. O.; Gural'skiy, I. A. Spin Crossover in Fe(II)–M(II) Cyanoheterobimetallic Frameworks (M = Ni, Pd, Pt) with 2-Substituted Pyrazines. *Inorg. Chem.* **2016**, *55*, 4906–4914.

(15) (a) Sheldrick, G. M. Crystal structure refinement with SHELXL. *Acta Crystallogr., Sect. C Struct. Chem.* **2015**, *71*, 3–8. (b) Dolomanov, O. V.; Bourhis, L. J.; Gildea, R. J.; Howard, J. A. K.; Puschmann, H. OLEX2: a complete structure solution, refinement and analysis program. *J. Appl. Crystallogr.*, **2009**, *42*, 339–341.

(16) (a) Gural'skiy, I. A.; Golub, B. O.; Shylin, S. I.; Ksenofontov, V.; Shepherd, H. J.; Raithby, P. R.; Tremel, W.; Fritsky, I. O. Cooperative High-Temperature Spin Crossover Accompanied by a Highly Anisotropic Structural Distortion. *Eur. J. Inorg. Chem.* **2016**, 3191–3195. (b) Gural'skiy, I. A.; Shylin, S. I.; Golub, B. O.; Ksenofontov, V.; Fritsky, I. O.; Tremel, W. High temperature spin crossover in [Fe(pyrazine){$Ag(CN)_2$}$_2$] and its solvate. *New J. Chem.* **2016**, *40*, 9012–9016.

(17) Brunner, H.; Tsuno, T.; Balazs, G.; Bodensteiner, M. Methyl/phenyl attraction by CH/π interaction in 1,2-substitution patterns. *J. Org. Chem.* **2014**, *79*, 11454–11462.

(18) (a) Reger, D. L.; Gardinier, J. R.; Smith, M. D.; Shahin, A. M.; Long, G. J.; Grandjean, F. Polymorphism in Fe[(*p*-IC_6H_4)B(3-Mepz)$_3$]$_2$ (pz = Pyrazolyl): Impact of Supramolecular Structure on an Iron(II) Electronic Spin-State Crossover. *Inorg. Chem.* **2005**, *44*, 1852–1866. (b) Reger, D. L.; Elgin, J. D.; Smith, M. D.; Grandjean, F.; Rebbouh, L.; Long, G. J. Structural identification of the factors that prevent an electronic spin-state crossover in Fe[(C_6H_5)B(3-Mepz)$_3$]$_2$ (pz = pyrazolyl ring). *Polyhedron* **2006**, *25*, 2616–2622.

(19) König, E.; Ritter, G.; Goodwin, H. A. Thermally induced incomplete high-spin ($^5T_2$) ⇌ low-spin ($^1A_1$) transition in solid bis[2-(2-pyridylamino)-4-(2-pyridyl) thiazolato]iron (II). *Chem. Phys.* **1974**, *5*, 211–223.

For Table of Contents Only

Using divalent iron, 2-methylpyrazine and dicyanometalates $[M(CN)_2]^-$ (M = Au, Ag) as building blocks, two Hofmann-like MOFs were obtained and characterized. Temperature-dependent changes in magnetic properties and Mössbauer spectra evidence a two-step spin transition in the Au-containing compound, while the Ag-based analog remains high-spin in the whole temperature range.